

Combination of AIBP, apoA-I, and Aflibercept Overcomes Anti-VEGF Resistance in Neovascular AMD by Inhibiting Arteriolar Choroidal Neovascularization

Zhao Zhang, Megan M. Shen, and Yingbin Fu

Cullen Eye Institute, Baylor College of Medicine, Houston, Texas, United States

Correspondence: Yingbin Fu, Cullen Eye Institute, One Baylor Plaza, Baylor College of Medicine, Neurosensory building, NC 506, Houston, TX 77030, USA; yingbin.fu@bcm.edu.

Received: June 3, 2022

Accepted: October 4, 2022

Published: November 1, 2022

Citation: Zhang Z, Shen MM, Fu Y. Combination of AIBP, apoA-I, and aflibercept overcomes anti-VEGF resistance in neovascular AMD by inhibiting arteriolar choroidal neovascularization. *Invest Ophthalmol Vis Sci.* 2022;63(12):2. <https://doi.org/10.1167/iovs.63.12.2>

PURPOSE. Anti-VEGF resistance represents a major unmet clinical need in the management of choroidal neovascularization (CNV). We have previously reported that a combination of AIBP, apoA-I, and an anti-VEGF antibody overcomes anti-VEGF resistance in laser-induced CNV in old mice in prevention experiments. The purpose of this work is to conduct a more clinically relevant study to assess the efficacy of the combination of AIBP, apoA-I, and aflibercept in the treatment of anti-VEGF resistance of experimental CNV at different time points after laser photocoagulation.

METHODS. To understand the pathobiology of anti-VEGF resistance, we performed comprehensive examinations of the vascular morphology of laser-induced CNV in young mice that are highly responsive to anti-VEGF treatment, and in old mice that are resistant to anti-VEGF therapy by indocyanine green angiography (ICGA), fluorescein angiography (FA), optical coherence tomography (OCT), and Alexa 568 isolectin labeled choroid flatmounts. We examined the efficacy of the combination therapy of AIBP, apoA-I, and aflibercept intravitreally delivered at 2, 4, and 7 days after laser photocoagulation in the treatment of CNV in old mice.

RESULTS. Laser-induced CNV in young and old mice exhibited cardinal features of capillary and arteriolar CNV, respectively. The combination therapy and the aflibercept monotherapy were equally effective in treating capillary CNV in young mice. In old mice, the combination therapy was effective in treating anti-VEGF resistance by potently inhibiting arteriolar CNV, whereas aflibercept monotherapy was ineffective.

CONCLUSIONS. Combination therapy of AIBP, apoA-I, and aflibercept overcomes anti-VEGF resistance in experimental CNV in old mice by inhibiting arteriolar CNV.

Keywords: choroidal neovascularization (CNV), apolipoprotein A-I binding protein (AIBP), anti-VEGF resistance, age-related macular degeneration (AMD), indocyanine green angiography (ICGA)

Age-related macular degeneration (AMD) is a major cause of blindness in the elderly that is rapidly increasing in prevalence with the aging of the population. In the United States, the number of patients with AMD is expected to increase substantially from 11 million to nearly 22 million by 2050, whereas the global prevalence is expected to increase to 288 million by the year 2040.¹ Choroidal neovascularization (CNV or wet AMD), which accounts for 10% to 20% of AMD, is responsible for 80% to 90% of blindness in patients with AMD.² Anti-vascular endothelial growth factor (VEGF) therapies that target extracellular VEGF have revolutionized the treatment of CNV. However, up to 50% of patients have suboptimal responses and outcomes to this treatment with evidence of persistent disease activity, such as persistent fluid and unresolved or new hemorrhage.³⁻⁷ The long-term outcomes can be suboptimal even among responders and can lead to anti-VEGF resistance.^{5,7-9} For example, 51.5% of patients receiving intravitreal ranibizumab and 67.4% of patients treated with bevacizumab had persistent fluid despite monthly treatment for 2 years (CATT trial).³ There

were 19.7% to 36.6% of patients who had active exudation after 1 year of regular 2.0 mg aflibercept treatments (VIEW 1 and VIEW 2 trials).¹⁰ The mean visual acuity gradually decreased during long-term follow-up with retreatment using a pro re nata (prn) regimen when patients exited from the MARINA or ANCHOR trial (SEVEN-UP study).⁵ Different strategies have been tested to overcome this issue, including increasing the frequency of anti-VEGF therapy and switching to different anti-VEGF agents. Various combination therapies have been explored in clinical trials, including targeting platelet-derived growth factor (PDGF; Fovista) and angiopoietin-2 (e.g. nesvacumab and faricimab). However, no major breakthroughs have been reported in combating anti-VEGF resistance. Thus, development of an effective therapy addressing anti-VEGF resistance represents an important unmet clinical need.

CNV is driven by abnormal levels of angiogenesis and inflammation, in which VEGF₁₆₅ (VEGF₁₆₄ in mice, we will use VEGF for simplicity hereafter), endothelial cells, and macrophages are critically involved. In particular,

accumulating evidence from both animal models and human patients suggests that macrophages play important roles in the pathogenesis of wet AMD.^{11–22} Specifically, dysregulation of macrophage cholesterol homeostasis has been implicated,^{20,23} and hyper-reflective lipid-filled macrophages or microglia have been detected in wet AMD.^{24–27} Notably, macrophages have increased density and proliferative activity in response to bevacizumab treatment, suggesting that macrophages play a role in anti-VEGF resistance.²⁸ These studies prompted us to explore a new treatment strategy for CNV by targeting VEGF, endothelial cells, and macrophages to address the limitations of current anti-VEGF monotherapy.

We and others reported that the secretory apolipoprotein A-I (apoA-I) binding protein (AIBP) enhances cholesterol efflux in endothelial cells and macrophages.^{29–32} AIBP binds its partner apoA-I or high-density lipoprotein (HDL) to enhance cholesterol efflux and inhibit lipid raft-anchored VEGFR2 signaling in endothelial cells.²⁹ By binding to the toll-like receptor 4 (TLR4), AIBP also augments cholesterol efflux from cholesterol-laden, inflamed macrophages/microglia, normalizes plasma lipid rafts, and suppresses inflammation.^{30,31,33,34} The unique properties of AIBP that target both endothelial cells and macrophages makes it an ideal drug candidate to work synergistically with anti-VEGF agents to treat CNV. Indeed, we recently found that a combination of AIBP, apoA-I, and an anti-VEGF neutralizing antibody eliminated anti-VEGF resistance and effectively suppressed CNV in mice when applied immediately after laser photocoagulation (i.e. prevention experiment).³²

To develop an effective therapy that addresses the limitation of current anti-VEGF treatments, it is essential to develop a clinically relevant animal model of CNV that is resistant to anti-VEGF treatment. Multiple pivotal clinical trials have shown that in human patients, advanced age and larger CNV lesions at baseline are associated with worse anti-VEGF treatment outcomes (e.g. ANCHOR, MARINA, and CATT studies).^{8,35–37} We found that laser photocoagulation produced larger CNV lesions in aged mice, that were much more resistant to anti-VEGF treatment compared with those in young mice.³² Furthermore, anti-VEGF resistance in patients with CNV is frequently associated with arteriolar CNV, which is characterized by large-caliber branching arterioles, vascular loops, and anastomotic connections.⁷ Recurrent anti-VEGF treatment can lead to vessel abnormalization, arteriolar CNV formation, and anti-VEGF resistance.^{9,38} On the other hand, anti-VEGF responders are characterized by having capillary CNV, in which leakage occurs because of VEGF-mediated permeability of leaky capillaries.

In this study, we performed comprehensive examination of laser-induced CNV in young and old mice by fluorescein angiography (FA), indocyanine green angiography (ICGA), spectral-domain optical coherence tomography (SD-OCT), and retinal pigment epithelium (RPE)-choroid flatmount imaging. We found that laser-induced CNV in young and old mice exhibits cardinal features of capillary and arteriolar CNV, respectively. We then performed a more clinically relevant experiment comparing the efficacy of AIBP/apoA-I/aflibercept combination therapy with the aflibercept monotherapy in the treatment of CNV in young and old mice at different time points after laser photocoagulation. Our data show that the combination therapy but not the aflibercept alone overcomes anti-VEGF resistance by potentially inhibiting arteriolar CNV.

METHODS

Mice

Wild type (WT; *C57BL/6J*) mice were purchased from Jackson Laboratory. *Naxe*^{-/-} mice (*C57BL/6N-A^{tm1Brd}* *Apoa1bp^{tm1a(EUCOMM)Hmgu}/BayMmucd*, RRID:MMRRC 041520-UCD) were obtained from the Mutant Mouse Resource and Research Center (MMRRC) at University of California at Davis. Old male and female *C57BL/6* mice (9–12 months) were ordered from the Comparative Medicine of Baylor College of Medicine and maintained in house until they reached the desired age (12–15 months for females and 16–18 months for males). We have shown previously that laser-induced CNV in both old male and female mice exhibit anti-VEGF resistance.³² All animal experiments were approved by the Institutional Animal Care and Use Committees (IACUC) at Baylor College of Medicine and were performed in accordance with the Association for Research in Vision and Ophthalmology (ARVO) Statement for the Use of Animals in Ophthalmic and Vision Research.

Laser-Induced Choroidal Neovascularization

Laser photocoagulation was carried out as described previously using the Micron IV retinal imaging system (Phoenix Research Lab, Pleasanton, CA, USA) with the Meridian Merilas 532 green laser (240 mW, 150 ms, and 50 μ m spot).³⁹ Four laser spots were generated per eye. *C57BL/6J* mice (6 to 9-week-old male and female mice and 12–15-month-old female mice) were used. At day 7 or 10 after laser treatment, CNV was analyzed by FA, ICGA, SD-OCT, and Alexa 568 isolectin B4 staining of RPE-choroidal flatmounts. Alexa 568 labeled lesion size was quantified by Image-Pro Plus (Media Cybernetics, Inc., Rockville, MD, USA). Unsuccessful laser burns without Bruch's membrane rupture were excluded. For three treatment groups (e.g. control, aflibercept, and combination) with an average maximum difference between area means of 37,000 and SD of 46,000 (arbitrary units from image measurement), the sample size is 31 laser spots for a standard power of 80% and alpha of 0.05 (one-way ANOVA).

Intravitreal Delivery

Intravitreal injection in mice was performed with an injection volume of 1.2 μ L as previously described.⁴⁰ A combination of 2.4 μ g AIBP, 4.8 μ g apoA-I, and 2 μ g aflibercept (combination therapy) or anti-VEGF monotherapy (2 μ g aflibercept and 7.2 μ g BSA) or control (7.2 μ g BSA and 2 μ g human IgG1 isotype control [Bio X cell, Lebanon, NH, USA]) were delivered by intravitreal injection at 2, 4, or 7 days after laser photocoagulation. AIBP was expressed as an N-terminal His-tagged protein in *E. coli* and purified by Ni-NTA chromatography following a standard protocol. ApoA-I was purified from human plasma by size exclusion chromatography as described.⁴¹ Aflibercept was from Regeneron Pharmaceuticals, Inc.

FA, ICGA, Funduscopy, and SD-OCT

For all in vivo imaging, mice were anesthetized by intraperitoneal injection of Ketamine (65–100 mg/kg) and Xylazine (10–20 mg/kg) per body weight. Pupils were dilated with 1% Tropicamide (Henry Schein Medical). Funduscopy examinations were performed with MICRON IV from Phoenix

Research Laboratories (San Ramon, CA, USA). FA, ICGA, and SD-OCT were taken with HRA-OCT device (Spectralis) from Heidelberg Engineering (Heidelberg, Germany). Indocyanine green (Pfaltz & Bauer, 2 mg/kg) and fluorescein sodium (AK-FLUOR, 10 mg/kg) were co-delivered into mice by tail vein injection or intraperitoneal (i.p.) injection. Immediately after injection, the time course of ICGA and FA were recorded. Because immune cells are readily labeled by ICG and accumulate in the laser spots over a period of 1 to 2 weeks following a single injection,⁴² which interferes with the imaging of CNV structure, each mouse eye was used to generate one data point for the ICGA timecourse of capillary and arteriolar CNV formation. OCT sessions were performed at 55 degrees field-of-view using the high-resolution mode (signal quality ≥ 35 dB). The focus depth was 10 to 20 D for combined OCT and ICGA. FA, ICGA, and SD-OCT data were exported as 8-bit grayscale image files. The degree of vascular permeability of each CNV lesion was quantified as the percentage increase in the area of fluorescence between the early and late phases of FA as described.⁴³ The retinal thickness in CNV lesion areas was measured from nerve fiber layer to RPE.^{44,45} Three to four measurements from different locations from each CNV lesion were taken.

Statistics

Statistics were calculated by the χ^2 test in Tables. For all figures, data were tested for normality using the Shapiro-Wilk normality test. Because one or more conditions failed the normality test in each data set, a Mann-Whitney test for two groups or Kruskal-Wallis test with Dunn's post hoc analysis for multiple groups was used for statistical comparison. The significance levels were marked by asterisks (*): * $P < 0.05$; ** $P < 0.01$; *** $P < 0.001$; and **** $P < 0.0001$. Bars represent mean \pm SD in all figures. Statistical significance (P value) was indicated in the figures and figure legends. Statistical analysis was performed with OriginPro or Graph-Pad Prism.

RESULTS

Characterization of CNV Lesion Types in Young and Old Mice by ICGA

Neovascular AMD in patients and animal models is typically examined by FA to reveal leakage patterns. However, because FA does not show the vascular morphology of CNV, we used ICGA,^{46,47} which allows penetration through the RPE due to the infrared spectrum of ICG, to characterize the lesion types of laser-induced CNV. Laser-induced CNV in young (7 to 9-week-old mice) mice predominantly exhibited capillary CNV (91.4%) as assessed by ICGA (Fig. 1A, Table 1). In contrast, 87.5% of CNV in old mice (18-month males or 12–15-month females) exhibited arteriolar CNV, characterized by large-caliber vessels with branching arterioles, vascu-

lar loops, and anastomotic connections.⁷ Indeed, although early phase ICGA readily detects large caliber vessels in arteriolar CNV (Fig. 1B, green circle), it could not resolve the fine capillary structure in young mice (see Fig. 1A, red circle). A large-caliber feeder vessel (red arrow) that gives rise to branching arterioles and terminal vascular anastomotic loops can be seen in CNV in old mice (Fig. 1C). These CNV patterns were confirmed by Alexa 568 isolectin labeled RPE-choroid flatmounts (Fig. 1D, arrowheads and arrows indicate branching arterioles and vascular loops in old mice, respectively). The CNV lesion area was increased 3.4 times ($P < 0.0001$) in old mice when compared with that of the young mice (Fig. 1E).

We performed ICGA at days 2, 4, 5, and 7 after laser photocoagulation in young and old mice. At day 2, ICGA revealed the formation of a ring-like structure in laser spots, reflecting the formation of a scaffold in both young and old mice (see Figs. 2A, 2B, red arrows). Minimal vasculature was detected in the center. At day 4, well-formed vasculature could be seen in the center in young mice (Fig. 2C, white arrow). The ring-like structure started to disappear. In old mice, the ring-like structure became more prominent (Fig. 2D, red arrows), and a large caliber vessel was formed across the ring (Fig. 2D, green arrows). At post-laser day 5 (P5), capillary CNV complex was largely finished, and the ring-like structure completely disappeared in young mice. In old mice, the ring-like structure largely disappeared, and was accompanied by the formation of a network of large caliber vessels. At P7, there is little change of the CNV complex in young mice. In old mice, arteriolar CNV consisting of branching arterioles and vascular anastomotic loops was formed. Our data suggest that capillary CNV in young mice developed more rapidly than arteriolar CNV in old mice.

Characterization of CNV Lesion Types in Young and Old Mice by FA

We examined the CNV in young and old mice by time course FA. The fluorescein dye filled in the arteriolar CNV in old mice more rapidly than the capillary CNV in young mice in the early phase FA (Fig. 3A). Old mice also exhibited profound leakage in the late phase FA (see Fig. 3A). To quantitatively compare the vascular permeability of CNV between young and old mice, we measured the change of fluorescent area between the early and late phases of FA.⁴³ Arteriolar CNV in old mice is associated with 2.3 times increased leakage (Fig. 3B, $P < 0.0001$). The arteriolar CNV in old mice is likely to produce increased leakage as a result of high rates of blood flow and poorly formed tight junctions at arteriovenous anastomotic loops.⁷

Characterization of CNV Lesion Types in Young and Old Mice by SD-OCT

Cross-sectional OCT scans of capillary CNV in young mice and arteriolar CNV in old mice showed very different features (Fig. 4A). Compared with capillary CNV, arteriolar CNV exhibited much larger subretinal fibro-vascular CNV membrane (dashed red line) with multiple compartment subretinal fluid (red arrows), consistent with the extensive leakage seen in FA (see Fig. 3). Retinal thickness in the lesion area in old mice was significantly increased (40% increase, $P < 0.0001$; Fig. 4B). In contrast, capillary CNV exhibited no subretinal fluid. RPE, outer nuclear layer (ONL), and outer plexiform layer (OPL) were disrupted in both CNV types.

TABLE 1. Distribution of Capillary and Arteriolar CNV in Young Versus Old Mice Based on ICGA

	Capillary	Arteriolar
Young	53 (91.4%)	5 (8.6%)
Old	8 (12.5%)	56 (87.5%)

Percentage in brackets represents row percentage; χ^2 (1, $N = 122$) = 75.7, $P < 0.001$.

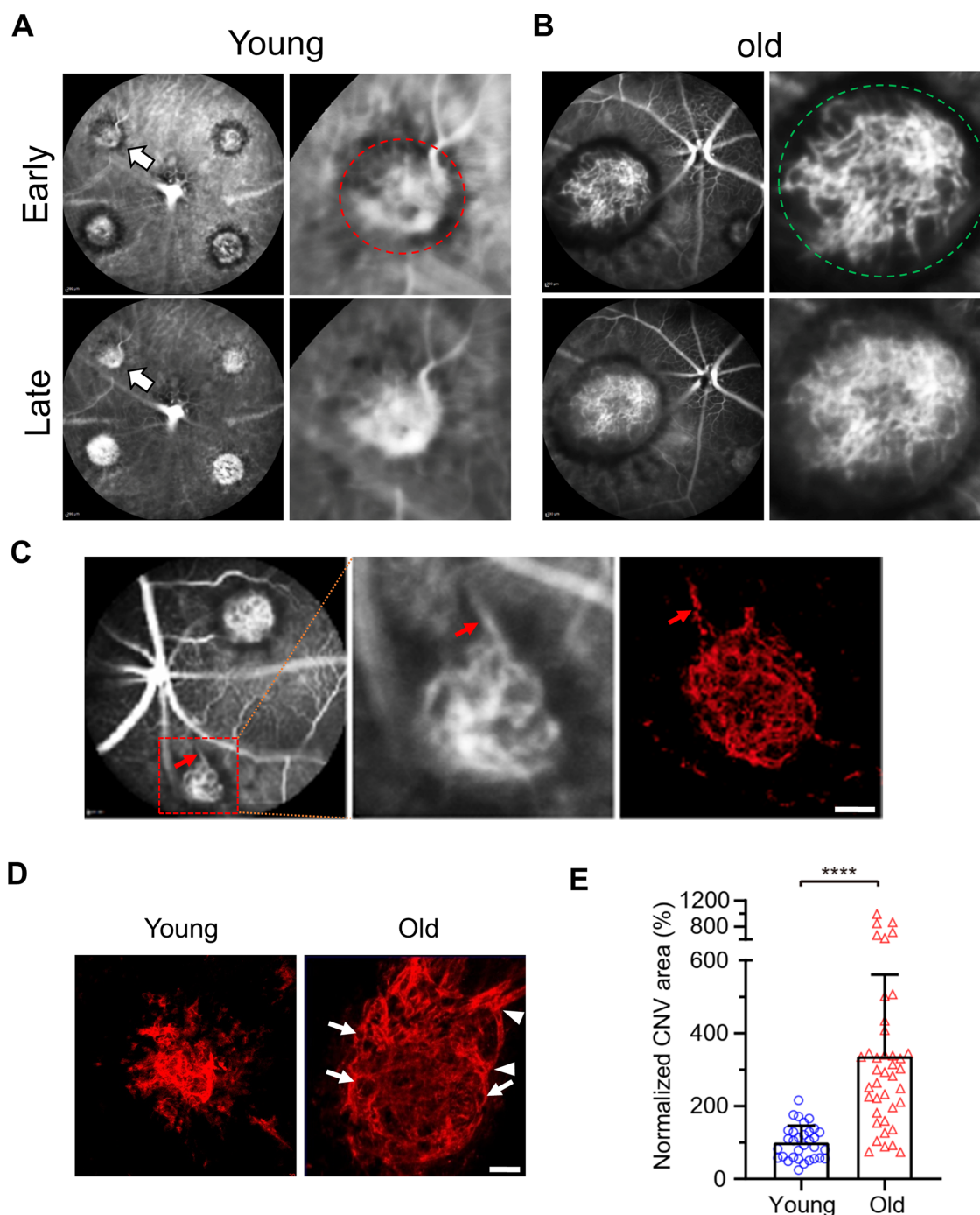


FIGURE 1. Vascular morphology of laser-induced CNV in young and old mice. (A) Early and late phase ICGA in laser-induced CNV in young mice. Magnified images of the lesion (*white arrows*) in the left were shown on the right. (B) Early and late phase ICGA in laser-induced CNV in old mice. Magnified images of the lesion in the left were shown on the right. (C) ICGA and the corresponding Alexa 568 isolectin labeled arteriolar CNV. The *middle panel* shows the magnified image of the lesion in the left (*red dashed square*). *Red arrows* indicate a large caliber feeder vessel. (D) Representative images of CNV lesions labeled by Alexa 568 isolectin on RPE/choroid flatmounts in young and old mice. *Arrowheads* and *arrows* indicate branching arterioles and vascular loops in old mice, respectively. Scale bar = 40 μ m. (E) Quantitative results of normalized CNV area in young and old mice. CNV areas were measured from Alexa 568 isolectin labeled RPE/choroid flatmounts. $N = 32$ and 40 laser spots in young and old mice, respectively. Bars represent mean \pm SD. ****, $P < 0.0001$.

Role of AIBP in Arteriolar CNV Formation

We determined the role of AIBP in the formation of capillary versus arteriolar CNV by a loss-of-function approach using the $Naxe^{-/-}$ ($Naxe$ encoding AIBP) mice. Compared with

young WT mice, young $Naxe^{-/-}$ mice showed increased arteriolar CNV formation (8.8% in young WT versus 32.5% in young $Naxe^{-/-}$ mice; Fig. 5A). Nevertheless, young $Naxe^{-/-}$ mice are still dominated by capillary CNV (67.5%) compared with only 12.5% capillary CNV in old WT mice. Our data

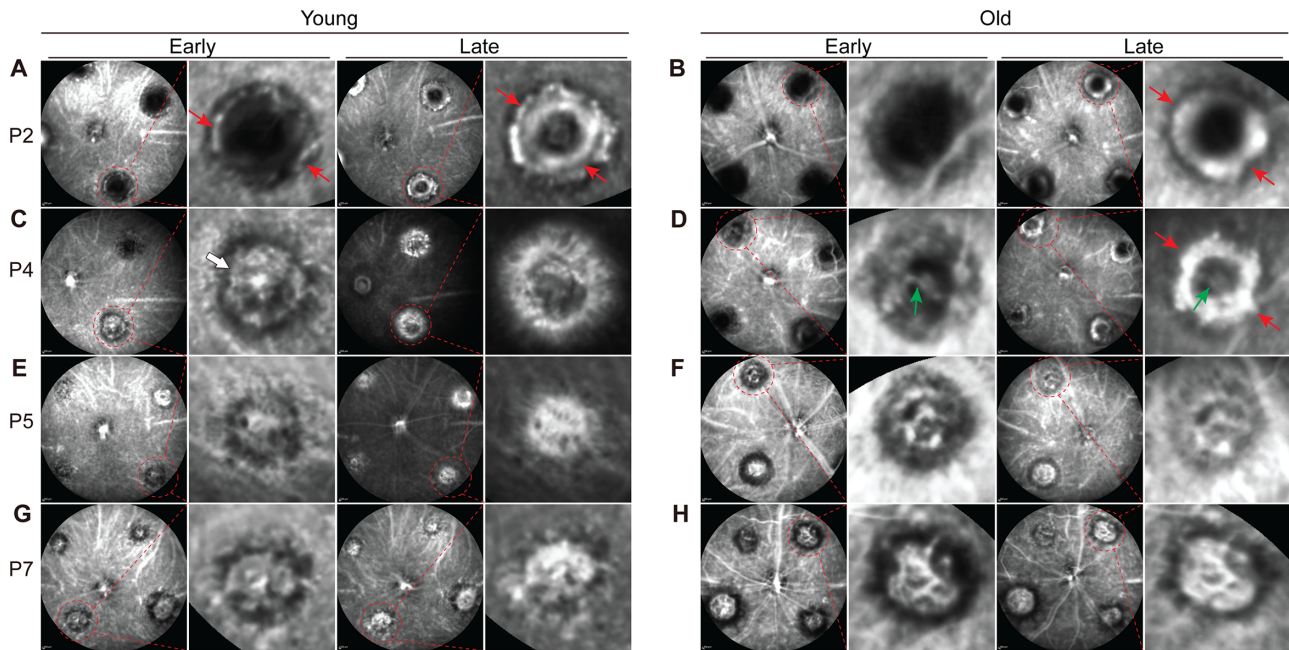


FIGURE 2. Timecourse of capillary and arteriolar CNV formation at days 2, 4, 5, and 7 after laser photocoagulation in young and old mice, respectively. CNV formation was imaged by ICGA. Each mouse eye was used to generate one data point. Red arrows indicate the formation of a ring-like scaffold in both young and old mice. The white arrow indicates well-formed vasculature in the center in young mice at day 4. The green arrows indicate the formation of a large caliber vessel across the ring in old mice at day 4.

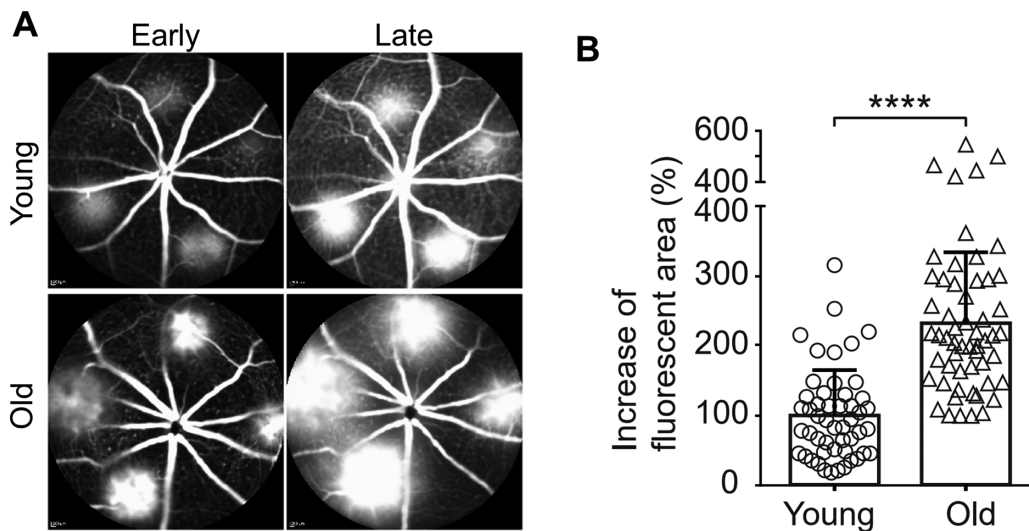


FIGURE 3. Laser-induced CNV in old mice exhibits significantly increased hyperpermeability compared with that in young mice. (A) Early and late phase FA in laser-induced CNV in young and old mice. (B) The percentage increase in the area of fluorescence in each CNV lesion between the early and late phases, indicating the degree of fluorescein leakage from the CNV, was calculated for each lesion and quantified. $N = 50$ and 56 laser spots in young and old mice, respectively. Bars represent mean \pm SD. ****, $P < 0.0001$.

suggest that AIBP does not play a major role in arteriolar CNV formation. Laser-induced CNV in young *Naxe*^{-/-} mice showed increased CNV area and leakage compared with young WT mice, but reduced CNV area and leakage compared with old WT mice (see Figs. 5B, 5C). In conjunction with previous studies,^{29,32,48} our data suggest that AIBP accelerates both capillary and arteriolar angiogenesis under physiological and pathological conditions.

Combination Therapy and Anti-VEGF Monotherapy are Equally Effective in the Treatment of Capillary CNV in Young Mice

We compared the efficacy of aflibercept with the combination of AIBP/apoA-I and aflibercept in the treatment of CNV in 6 to 9-week-old young mice. We previously reported that a combination of $2.4 \mu\text{g}$ AIBP and $10 \mu\text{g}$ apoA-I conferred

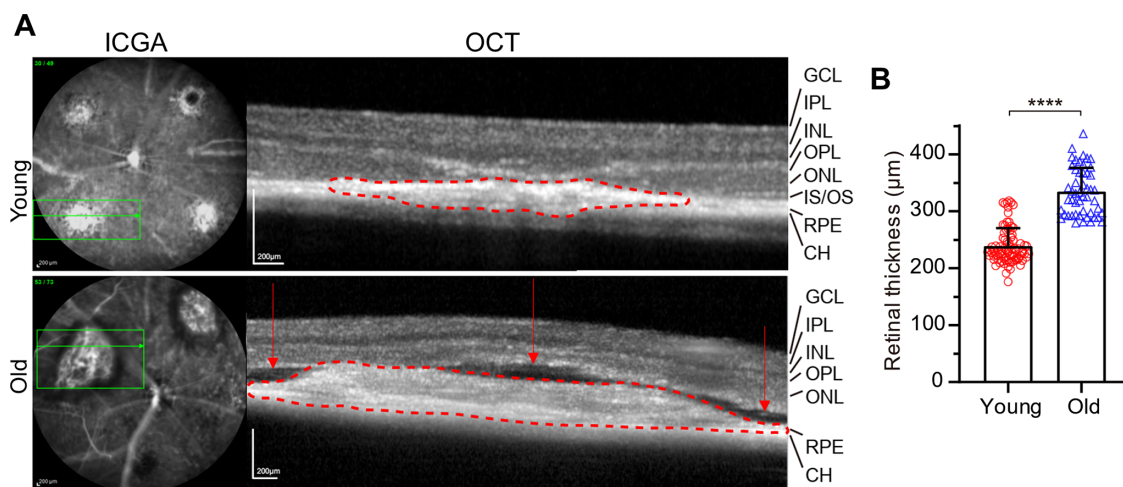


FIGURE 4. SD-OCT imaging of CNV pathology in young and old mice. (A) Green horizontal line in ICGA indicates the OCT scanning position. Choroidal fibro-vascular tissue was marked by the *red dotted lines*. The *red arrows* indicate compartment subretinal fluid in old mice. **(B)** Quantitative results of retinal thickness in CNV lesion area in young and old mice. $N = 84$ measurements from 27 laser spots from young mice and 50 measurements from 16 laser spots from old mice. Bars represent mean \pm SD. ****, $P < 0.0001$.

maximal inhibition of CNV in mice.³² Subsequently, we found that maximal inhibition could be achieved using 2.4 μg AIBP and 4.8 μg apoA-I (Supplementary Fig. S1). The clinical dose of aflibercept is 2 mg/human eye, and human vitreous volume of 4.6 to 5.0 mL⁴⁹ is approximately 1000 times that of the mouse (5 μL).⁵⁰ Thus, we used 2 μg (i.e. 2 mg/1000) aflibercept in this study, a level previously described to be optimal in mice.⁵¹ A combination of 2.4 μg AIBP, 4.8 μg apoA-I, and 2 μg aflibercept or 2 μg aflibercept alone was administered in 6 to 9-week-old mice at day 2 after laser photocoagulation. Seven days after the laser, CNV leakage was assessed by FA, whereas the CNV area was visualized by Alexa-568 isolectin labeled RPE-choroid flatmounts. The combination treatment was equally effective as the aflibercept monotherapy in reducing CNV leakage (23% reduction) and in reducing the CNV area (approximately 45% reduction) of lesions in young mice that were dominated by capillary CNV (Figs. 6A–D).

Combination Therapy Overcomes Anti-VEGF Resistance by Suppressing Arteriolar CNV

We have shown previously that a combination of AIBP/apoA-I and an anti-VEGF antibody delivered immediately after laser photocoagulation (i.e. prevention) overcame anti-VEGF resistance in old mice.³² In this experiment, we examined the efficacy of a combination of 2.4 μg AIBP, 4.8 μg apoA-I, and 2 μg aflibercept intravitreally delivered at 2 and 4 days after laser photocoagulation in the treatment of CNV in old mice. At both treatment time points, the AIBP/apoA-I/aflibercept combination therapy significantly inhibited arteriolar CNV formation (Figs. 7A, 7B, white dashed line). These lesions were converted into a mixed-type CNV (see Figs. 7A, 7B, green dashed line; i.e. smaller CNV size with less prominent arteriolar CNV features [large-caliber vessels with branching arterioles, vascular loops, etc.]) and contain capillary CNV (Table 2). Combination therapy significantly reduced both the CNV leakage (42%, $P < 0.001$ and 59%, $P < 0.0001$ reduction for P2 and P4 treatment, respectively) and the CNV area (29%,

$P < 0.05$ and 45%, $P < 0.01$ reduction for P2 and P4 treatment, respectively; Figs. 7C–F). In sharp contrast, aflibercept monotherapy had no effect in inhibiting arteriolar CNV (see Figs. 7A, 7B, yellow dashed line; Tables 2, 3) or reducing CNV leakage or area (Figs. 7C–F). Because arteriolar CNV was not completely formed until day 7 after laser photocoagulation (see Fig. 2), we performed combination therapy at day 7 after laser treatment in old mice and analyzed at day 10. Combination therapy significantly reduced the number of arteriolar CNV (Table 4) and significantly reduced the CNV leakage (38.5% reduction, $P < 0.0001$; Fig. 7G). However, combination therapy did not significantly reduce the CNV size (Fig. 7H). We did not include aflibercept at P7 treatment because aflibercept showed no benefit even at P2 and P4 treatment. Because the role of aflibercept in reducing VEGF-dependent leakage from capillary CNV is well established (see Fig. 6C),^{52,53} the most parsimonious explanation of the persistent leakage despite aflibercept treatment is that arteriolar CNV causes anti-VEGF resistance (see Figs. 7C, 7E). This experiment suggests that AIBP/apoA-I/aflibercept combination overcomes anti-VEGF resistance by inhibiting arteriolar CNV.

DISCUSSION

The most important finding of this study is that combination therapy of AIBP, apoA-I, and aflibercept overcomes anti-VEGF resistance to aflibercept in experimental CNV in old mice by robustly inhibiting arteriolar CNV. By performing comprehensive in vivo imaging and choroid flatmount analysis, we show that the combination therapy significantly reduces both CNV leakage and size whereas aflibercept monotherapy is ineffective when the treatment was performed at either P2 or P4 after laser photocoagulation. When the treatment was performed at P7, combination therapy significantly reduced the CNV leakage, but not the CNV size. One possible explanation is that it requires longer treatment duration to cause the regression of arteriolar CNV with a network of large caliber vessels. This is difficult to achieve using the short-term laser-induced CNV mouse model, not to mention the short half-time and residence time of

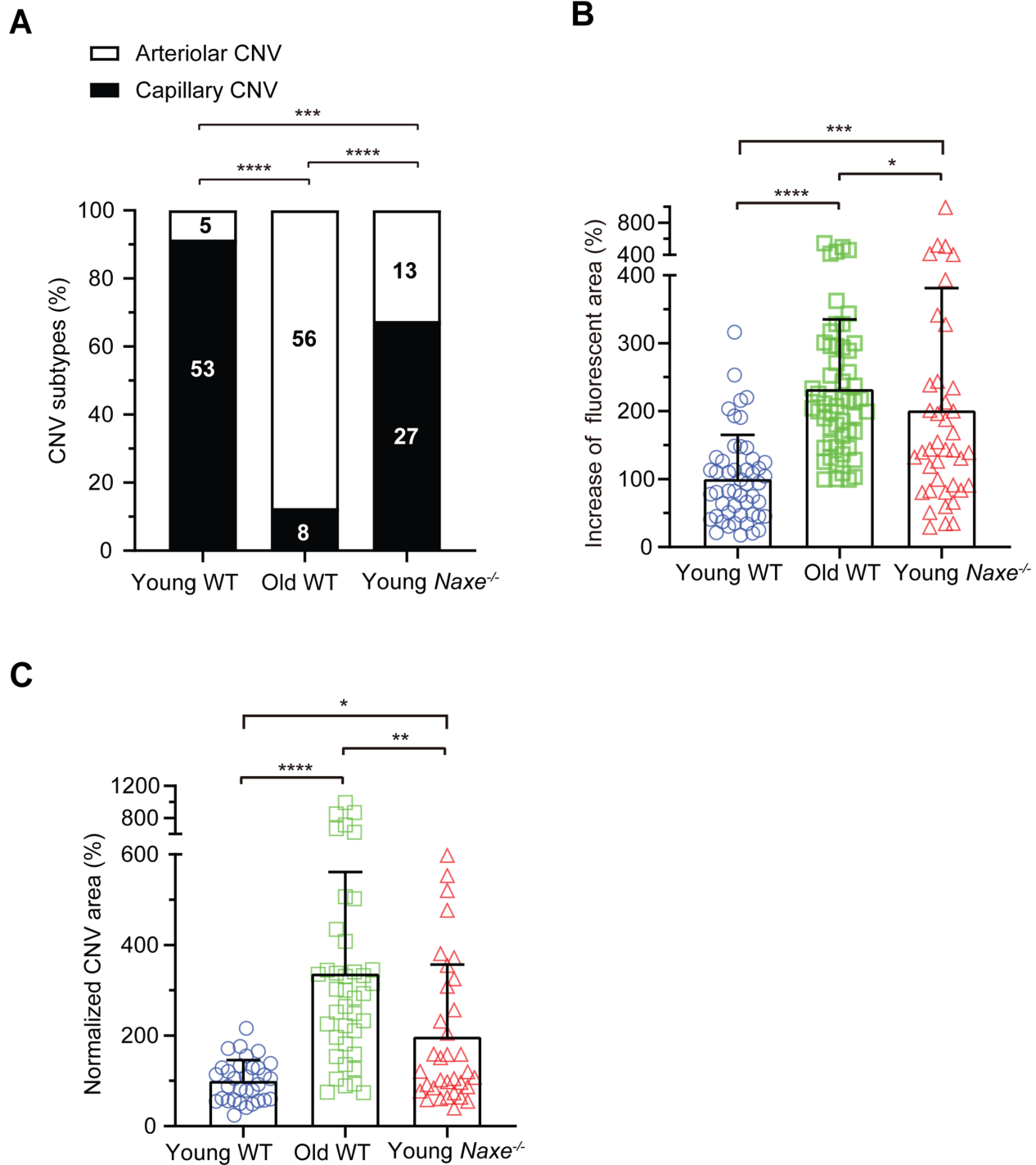


FIGURE 5. Comparison of CNV features in young WT, old WT, and young *Naxe*^{-/-} mice. (A) Distribution of capillary and arteriolar CNV in young WT, old WT, and young *Naxe*^{-/-} mice based on ICGA. Numbers inside the column indicate the number of laser spots. Statistical analysis was calculated by the χ^2 test. (B) The percentage increase of fluorescent area in each CNV lesion between the early and late phases of FA in young WT, old WT, and young *Naxe*^{-/-} mice. $N = 50$ (young WT), 56 (old WT), and 40 (young *Naxe*^{-/-}) laser spots. (C) Quantitative results of normalized CNV area in young WT, old WT, and young *Naxe*^{-/-} mice. CNV areas were measured from Alexa 568 isolectin labeled RPE/choroid flatmounts. $N = 32$ (young WT), 40 (old WT), and 34 (young *Naxe*^{-/-}) laser spots. Young WT (6–9 weeks), old WT (12 to 15-month-old female) mice, young *Naxe*^{-/-} mice (8–12 weeks) were subjected to laser photocoagulation and analyzed at day 7 after laser treatment. Statistical analysis in B and C was performed by Kruskal-Wallis test with Dunn's post hoc analysis. Bars represent mean \pm SD. *, $P < 0.05$; ***, $P < 0.001$; ****, $P < 0.0001$.

therapeutics in mouse eyes.⁵⁰ This issue will be better addressed using a recently developed rabbit CNV model that is resistant to the anti-VEGF treatment.⁵⁴ The much larger

eye size, longer half-time and residence time of therapeutics, and the possibility of repeated intravitreal injection (as in the case of human eyes) makes the rabbit model ideal to test the

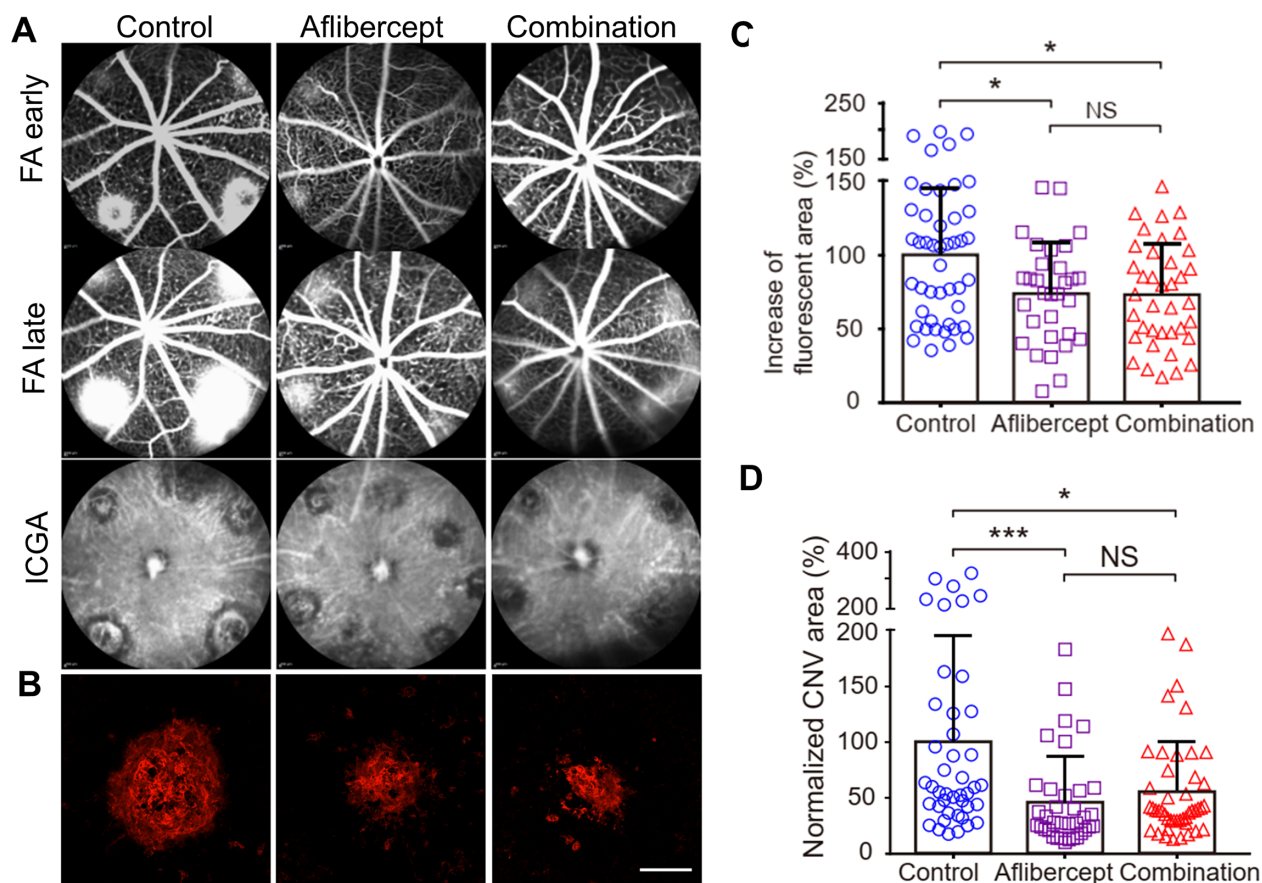


FIGURE 6. Comparison between aflibercept and combination therapy (AIBP, apoA-I, and aflibercept) in suppressing laser-induced CNV in young mice. (A) Representative images of FA (early and late phase) and ICGA of CNV lesions after different treatments. Therapeutics were delivered at day 2 after laser photocoagulation and analyzed at day 7. Some of the spots in the aflibercept treated eye were not laser spots but may reflect some issues of the choroidal vasculature of that particular eye (see Supplementary Fig. S2 for details). (B) Representative images of Alexa 568 isolectin labeled RPE/choroid flatmounts after treatments. (C) Quantitative results of the percentage increase of fluorescent area in each CNV lesion between the early and late phases of FA in A. $N = 45$ (control), 31 (aflibercept), and 38 (combination) laser spots. (D) Quantitative results of normalized CNV area in B. $N = 43$ (control), 36 (aflibercept), and 45 (combination) laser spots. Young mice (6–9 weeks) were treated at day 2 after laser photocoagulation. Statistical analysis in C and D was performed by Kruskal-Wallis test with Dunn's post hoc analysis. Bars represent mean \pm SD. NS, $P > 0.05$; *, $P < 0.05$; ***, $P < 0.001$.

therapeutic efficacy of the combination therapy as well as for pharmacokinetic studies. Future research will answer these important questions in preparation for an Investigational New Drug (IND) application. Nevertheless, by converting the arteriolar CNV from active exudation to a more quiescent stage, combination therapy offers significant therapeutic advantage in comparison to aflibercept alone.

Because the underlying pathobiology of anti-VEGF resistance is largely unknown, we compared the CNV phenotype of laser-induced CNV in young and old mice by comprehensive in vivo imaging (i.e. ICGA, FA, and OCT). We found that young mice predominantly develop capillary type CNV whereas old mice develop arteriolar CNV, consistent with previous findings based on choroid flatmount imaging of CNV vessel types.⁷ The vascular morphology of CNV can be readily detected by ICGA and confirmed by Alexa 568 isolectin labeled RPE-choroid flatmounts. To our knowledge, this is the first time ICGA has been applied to examine vascular morphology of CNV in animal models. FA shows that capillary CNV in young mice typically exhibit small lesions, well-demarcated borders, and mild fluorescein leakage while arteriolar CNV in old mice show large, confluent CNV with profound active fluorescein leakage. These

features are similar to those observed by ICGA in patients with neovascular AMD.⁷ Although the mechanism for arteriolar CNV formation is unknown, our hypothesis is that it shares features with arteriogenesis, whereas capillary CNV formation is similar to angiogenesis, in which new capillary blood vessels sprout from a preexisting blood vessel. Although angiogenesis is highly VEGF dependent, arteriogenesis is not VEGF dependent.^{55–57} In support of this hypothesis, we found that capillary CNV in young mice is highly responsive to aflibercept treatment, whereas arteriolar CNV in old mice is completely resistant to aflibercept treatment. These findings are consistent with clinical findings that anti-VEGF resistance in patients with CNV is frequently associated with arteriolar CNV while anti-VEGF responders are associated with capillary CNV.⁷ Furthermore, recurrent anti-VEGF treatment can lead to vessel abnormalization and arteriolar CNV formation, which then can lead to anti-VEGF resistance.^{9,38} These studies provide clinical relevance of using experimental CNV in old animals to model anti-VEGF resistance.

It is well established that monocytes and macrophages play a pivotal role in arteriogenesis by releasing growth factors, proteases, and chemokines, hence mediating cell

treatment in **G**. (**D**, **F**, **H**) Quantitative results of normalized CNV area. $N = 59$ (control), 34 (aflibercept), and 57 (combination) laser spots in **D**. $N = 36$ (control), 34 (aflibercept), and 38 (combination) laser spots in **F**. $N = 42$ (control) and 40 (combination) laser spots in **H**. Old female mice (12–15 months) were treated at day 2 (**A** through **D**), day 4 (**E** and **F**), and day 7 (**G**, and **H**) after laser photocoagulation and were analyzed at day 7 (**A** through **F**) and day 10 (**G** and **H**). Statistical analysis (**C** through **F**) was performed by Kruskal-Wallis test with Dunn's post hoc analysis. Bars represent mean \pm SD. NS, $P > 0.05$; *, $P < 0.05$; **, $P < 0.01$; ***, $P < 0.001$; ****, $P < 0.0001$. White and green dashed line indicates arteriolar CNV in control and aflibercept treated mice. Green dashed line indicates mixed type CNV in **A** and **B**.

TABLE 2. CNV Vessel Type Quantification in Old Mice After Different Treatments Based on Isolectin-B4 Staining (P2 Treatment)

	Arteriolar CNV	Mixed CNV	P Value
Control	49 (84.5%)	9 (15.5%)	
Aflibercept	27 (77.1%)	8 (22.9%)	0.375
AIBP + apoA-I + aflibercept	25 (44.6%)	31 (55.4%)	< 0.0001

Arteriolar CNV refers to CNV with prominent branching arterioles and vascular loops. Mixed CNV refers to smaller size CNV with less prominent arteriolar CNV features and that contains capillary CNV. See **Figures 7A** and **7B** CNV type in white and yellow dashed line (arteriolar CNV) and green dashed line (mixed CNV) as examples. Statistics were calculated by the χ^2 test. Percentage in brackets represents row percentage.

TABLE 3. CNV Vessel Type Quantification in Old Mice After Different Treatments Based on Isolectin-B4 Staining (P4 Treatment)

	Arteriolar CNV	Mixed CNV	P Value
Control	23 (74.2%)	8 (25.8%)	
Aflibercept	26 (74.3%)	9 (25.7%)	0.993
AIBP + apoA-I + aflibercept	15 (38.5%)	24 (61.5%)	0.00287

Statistics were calculated by the χ^2 test. Percentage in brackets represents row percentage.

TABLE 4. CNV Vessel Type Quantification in Old Mice After Different Treatments Based on Isolectin-B4 Staining (P7 Treatment)

	Arteriolar CNV	Mixed CNV	P Value
Control	31 (75.6%)	10 (24.4%)	
AIBP + apoA-I + aflibercept	21 (53.8%)	18 (46.1%)	0.0413

Statistics were calculated by the χ^2 test. Percentage in brackets represents row percentage.

proliferation and migration as well as structural remodeling of the extracellular compartment.^{58–61} Indeed, macrophage depletion in old mice converted arteriolar CNV to capillary CNV⁷ and restored CNV sensitivity to anti-VEGF treatment.³² Importantly, we show that the combination therapy is effective in elimination of anti-VEGF resistance by inhibiting arteriolar CNV. This is achieved by simultaneously targeting inflammatory macrophages with AIBP/apoA-I and neutralizing extracellular VEGF with aflibercept. Both AIBP and anti-VEGF agents target VEGFR2 signaling in endothelial cells,^{29,48} so why is the combination therapy synergistic? The likely answer is that VEGF is a pro-inflammatory cytokine that recruits macrophages, and at the same time, inflamed macrophages express more VEGF and other pro-angiogenic factors, creating a positive feedback loop.^{62–64} Thus, both anti-VEGF agents and AIBP may be required to interrupt this vicious cycle of events initiated by the reciprocal causal nexus of VEGF and inflammation.

We have shown previously that the combination of AIBP, apoA-I, and a VEGF neutralizing antibody is effective in over-

coming anti-VEGF resistance in prevention experiments (i.e. delivery immediately after laser).³² In this work, we demonstrated that a combination of AIBP, apoA-I, and aflibercept is effective in eliminating anti-VEGF resistance in treatment experiments (i.e. delivery at 2, 4, and 7 days after laser and analyzed at days 7 or 10), making it one step closer to clinical trials of the combination therapy. Because the long-term efficacy of anti-VEGF therapy is suboptimal and repeated anti-VEGF treatment can lead to arteriolar CNV and anti-VEGF resistance,^{9,38} we predict that the AIBP/apoA-I/anti-VEGF combination therapy will not only overcome anti-VEGF resistance for monotherapy nonresponders, but also improve therapeutic efficacy at all levels of anti-VEGF response in the treatment of neovascular AMD.

Acknowledgments

The authors thank Longhou Fang for providing AIBP, Wei Li for providing aflibercept, and Henry J. Pownall for providing human apoA-I. The *Naxe*^{-/-} mouse strain (C57BL/6N-*A^{tm1}Brd* *Apoa1bp*^{*tm1a*(EUCOMM)Hmgu}/BayMmucd, RRID:MMRRC 041520-UCD) used for this research project was obtained from the Mutant Mouse Resource and Research Center (MMRRC) at University of California at Davis, an National Institutes of Health (NIH)-funded strain repository, and was donated to the MMRRC by Arthur Beaudet, MD, Baylor College of Medicine. Mice were generated at the Baylor College of Medicine as part of the Baylor College of Medicine, Sanger Institute, and MRC Harwell (BaSH) Consortium for the NIH Common Fund program for Knockout Mouse Production and Cryopreservation (1U42RR033192-01) and Knockout Mouse Phenotyping (1U54HG006348-01).

Supported by grants from BrightFocus Foundation, Retinal Research Foundation, Mullen Foundation, the Sarah Campbell Blaffer Endowment in Ophthalmology (Y.F.), NIH core grant 2P30EY002520 to Baylor College of Medicine, and an unrestricted grant to the Department of Ophthalmology at Baylor College of Medicine from Research to Prevent Blindness.

Disclosure: **Z. Zhang**, None; **M.M. Shen**, None; **Y. Fu**, None

References

- Wong WL, Su X, Li X, et al. Global prevalence of age-related macular degeneration and disease burden projection for 2020 and 2040: a systematic review and meta-analysis. *Lancet Glob Health*. 2014;2:e106–e116.
- Bressler NM, Bressler SB, Fine SL. Age-related macular degeneration. *Surv Ophthalmol*. 1988;32:375–413.
- Comparison of Age-related Macular Degeneration Treatments Trials (CATT) Research Group, Maguire MG, Martin DF, et al. Five-Year Outcomes with Anti-Vascular Endothelial Growth Factor Treatment of Neovascular Age-Related Macular Degeneration: The Comparison of Age-Related Macular Degeneration Treatments Trials. *Ophthalmology*. 2016;123:1751–1761.
- Yang S, Zhao J, Sun X. Resistance to anti-VEGF therapy in neovascular age-related macular degeneration: a comprehensive review. *Drug Des Devel Ther*. 2016;10:1857–1867.

5. Rofagha S, Bhisitkul RB, Boyer DS, Sadda SR, Zhang, SEVEN-UP Study Group. Seven-year outcomes in ranibizumab-treated patients in ANCHOR, MARINA, and HORIZON: a multicenter cohort study (SEVEN-UP). *Ophthalmology*. 2013;120:2292–2299.
6. Krebs I, Glittenberg C, Ansari-Shahrezaei S, Hagen S, Steiner I, Binder S. Non-responders to treatment with antagonists of vascular endothelial growth factor in age-related macular degeneration. *Br J Ophthalmol*. 2013;97:1443–1446.
7. Mettu PS, Allingham MJ, Cousins SW. Incomplete response to Anti-VEGF therapy in neovascular AMD: Exploring disease mechanisms and therapeutic opportunities. *Prog Retin Eye Res*. 2021;82:100906.
8. Rosenfeld PJ, Shapiro H, Tuomi L, et al. Characteristics of Patients Losing Vision after 2 Years of Monthly Dosing in the Phase III Ranibizumab Clinical Trials. *Ophthalmology*. 2011;118:523–530.
9. Spaide RF. Optical Coherence Tomography Angiography Signs of Vascular Abnormalization With Antiangiogenic Therapy for Choroidal Neovascularization. *Am J Ophthalmol*. 2015;160:6–16.
10. Heier JS, Brown DM, Chong V, et al. Intravitreal aflibercept (VEGF trap-eye) in wet age-related macular degeneration. *Ophthalmology*. 2012;119:2537–2548.
11. Apte RS, Richter J, Herndon J, Ferguson TA. Macrophages inhibit neovascularization in a murine model of age-related macular degeneration. *PLoS Med*. 2006;3:e310.
12. Cherepanoff S, McMenamin P, Gillies MC, Kettle E, Sarks SH. Bruch's membrane and choroidal macrophages in early and advanced age-related macular degeneration. *Br J Ophthalmol*. 2010;94:918–925.
13. Espinosa-Heidmann DG, Suner IJ, Hernandez EP, Monroy D, Csaky KG, Cousins SW. Macrophage depletion diminishes lesion size and severity in experimental choroidal neovascularization. *Invest Ophthalmol Vis Sci*. 2003;44:3586–3592.
14. Grossniklaus HE, Ling JX, Wallace TM, et al. Macrophage and retinal pigment epithelium expression of angiogenic cytokines in choroidal neovascularization. *Mol Vis*. 2002;8:119–126.
15. Hagbi-Levi S, Grunin M, Jaouni T, et al. Proangiogenic characteristics of activated macrophages from patients with age-related macular degeneration. *Neurobiol Aging*. 2017;51:71–82.
16. Killingsworth MC, Sarks JP, Sarks SH. Macrophages related to Bruch's membrane in age-related macular degeneration. *Eye (Lond)*. 1990;4(Pt 4):613–621.
17. Lopez PF, Lambert HM, Grossniklaus HE, Sternberg P. Well-defined subfoveal choroidal neovascular membranes in age-related macular degeneration. *Ophthalmology*. 1993;100:415–422.
18. Sakurai E, Anand A, Ambati BK, van Rooijen N, Ambati J. Macrophage depletion inhibits experimental choroidal neovascularization. *Invest Ophthalmol Vis Sci*. 2003;44:3578–85.
19. Sarks JP, Sarks SH, Killingsworth MC. Morphology of early choroidal neovascularisation in age-related macular degeneration: correlation with activity. *Eye (Lond)*. 1997;11(Pt 4):515–522.
20. Sene A, Khan AA, Cox D, et al. Impaired cholesterol efflux in senescent macrophages promotes age-related macular degeneration. *Cell Metab*. 2013;17:549–561.
21. Subhi Y, Nielsen MK, Molbech CR, et al. Association of CD11b+ Monocytes and Anti-Vascular Endothelial Growth Factor Injections in Treatment of Neovascular Age-Related Macular Degeneration and Polypoidal Choroidal Vasculopathy. *JAMA Ophthalmol*. 2019;137:515–522.
22. Cousins SW, Espinosa-Heidmann DG, Csaky KG. Monocyte activation in patients with age-related macular degeneration: a biomarker of risk for choroidal neovascularization? *Arch Ophthalmol*. 2004;122:1013–1018.
23. Lin JB, Sene A, Santeford A, et al. Oxysterol Signatures Distinguish Age-Related Macular Degeneration from Physiologic Aging. *EBioMedicine*. 2018;32:9–20.
24. Pang CE, Messinger JD, Zanzottera EC, Freund KB, Curcio CA. The Onion Sign in Neovascular Age-Related Macular Degeneration Represents Cholesterol Crystals. *Ophthalmology*. 2015;122:2316–2326.
25. Li M, Dolz-Marco R, Messinger JD, et al. Clinicopathologic Correlation of Anti-Vascular Endothelial Growth Factor-Treated Type 3 Neovascularization in Age-Related Macular Degeneration. *Ophthalmology*. 2018;125:276–287.
26. Coscas G, De Benedetto U, Coscas F, et al. Hyperreflective dots: a new spectral-domain optical coherence tomography entity for follow-up and prognosis in exudative age-related macular degeneration. *Ophthalmologica*. 2013;229:32–37.
27. Kamei M, Yoneda K, Kume N, et al. Scavenger receptors for oxidized lipoprotein in age-related macular degeneration. *Invest Ophthalmol Vis Sci*. 2007;48:1801–1807.
28. Tatar O, Yoeruek E, Szurman P, et al. Effect of bevacizumab on inflammation and proliferation in human choroidal neovascularization. *Arch Ophthalmol*. 2008;126:782–790.
29. Fang L, Choi SH, Baek JS, et al. Control of angiogenesis by AIBP-mediated cholesterol efflux. *Nature*. 2013;498:118–122.
30. Schneider DA, Choi S-H, Agatista-Boyle C, et al. AIBP protects against metabolic abnormalities and atherosclerosis. *J Lipid Res*. 2018;59(5):854–863.
31. Zhang M, Zhao G-J, Yao F, et al. AIBP reduces atherosclerosis by promoting reverse cholesterol transport and ameliorating inflammation in apoE^{-/-} mice. *Atherosclerosis*. 2018;273:122–130.
32. Zhu L, Parker M, Enemchukwu N, et al. Combination of apolipoprotein-A-I/apolipoprotein-A-I binding protein and anti-VEGF treatment overcomes anti-VEGF resistance in choroidal neovascularization in mice. *Commun Biol*. 2020;3:386.
33. Woller SA, Choi S-H, An EJ, et al. Inhibition of Neuroinflammation by AIBP: Spinal Effects upon Facilitated Pain States. *Cell Rep*. 2018;23:2667–2677.
34. Navia-Pelaez JM, Choi S-H, Dos Santos Aggum Capetini L, et al. Normalization of cholesterol metabolism in spinal microglia alleviates neuropathic pain. *J Exp Med*. 2021;218(7):e20202059.
35. Kaiser PK, brown DM, Zhang K, et al. Ranibizumab for predominantly classic neovascular age-related macular degeneration: subgroup analysis of first-year ANCHOR results. *Am J Ophthalmol*. 2007;144:850–857.
36. Finger RP, Wickremasinghe SS, Baird PN, Guymer RH. Predictors of anti-VEGF treatment response in neovascular age-related macular degeneration. *Surv Ophthalmol*. 2014;59:1–18.
37. Boyer DS, Antoszyuk AN, Awh CC, et al. Subgroup analysis of the MARINA study of ranibizumab in neovascular age-related macular degeneration. *Ophthalmology*. 2007;114:246–252.
38. Lumbroso B, Rispoli M, Savastano MC, Jia Y, Tan O, Huang D. Optical Coherence Tomography Angiography Study of Choroidal Neovascularization Early Response after Treatment. *Dev Ophthalmol*. 2016;56:77–85.
39. Gong Y, Li J, Sun Y, et al. Optimization of an Image-Guided Laser-Induced Choroidal Neovascularization Model in Mice. *PLoS One*. 2015;10:e0132643.
40. Kumar S, Nakashizuka H, Jones A, et al. Proteolytic Degradation and Inflammation Play Critical Roles in Polypoidal Choroidal Vasculopathy. *Am J Pathol*. 2017;187:2841–2857.

41. Brewer HB, Ronan R, Meng M, Bishop C. Isolation and characterization of apolipoproteins A-I, A-II, and A-IV. *Methods Enzymol.* 1986;128:223–246.
42. Sim DA, Chu CJ, Selvam S, et al. A simple method for in vivo labelling of infiltrating leukocytes in the mouse retina using indocyanine green dye. *Dis Model Mech.* 2015;8:1479–1487.
43. Balaggan KS, Binley K, Esapa M, et al. EIAV vector-mediated delivery of endostatin or angiostatin inhibits angiogenesis and vascular hyperpermeability in experimental CNV. *Gene Ther.* 2006;13:1153–1165.
44. Giani A, Thanos A, Roh MI, et al. In Vivo Evaluation of Laser-Induced Choroidal Neovascularization Using Spectral-Domain Optical Coherence Tomography. *Invest Ophthalmol Vis Sci.* 2011;52:3880–3887.
45. Ragauskas S, Kielczewski E, Vance J, Kaja S, Kalesnykas G. In Vivo Multimodal Imaging and Analysis of Mouse Laser-Induced Choroidal Neovascularization Model. *J Vis Exp.* 2018;(131):56173.
46. Kumar S, Berriochoa Z, Jones AD, Fu Y. Detecting abnormalities in choroidal vasculature in a mouse model of age-related macular degeneration by time-course indocyanine green angiography. *J Vis Exp.* 2014;84:e51061.
47. Kumar S, Berriochoa Z, Ambati BK, Fu Y. Angiographic features of transgenic mice with increased expression of human serine protease HTRA1 in retinal pigment epithelium. *Invest Ophthalmol Vis Sci.* 2014;55:3842–3850.
48. Mao R, Meng S, Gu Q, et al. AIBP Limits Angiogenesis Through γ -Secretase-Mediated Upregulation of Notch Signaling. *Circ Res.* 2017;120:1727–1739.
49. Azhdam AM, Goldberg RA, Ugradar S. In Vivo Measurement of the Human Vitreous Chamber Volume Using Computed Tomography Imaging of 100 Eyes. *Translational Vision Science & Technology.* 2020;9:2.
50. Schmitt M, Hippeläinen E, Raviña M, et al. Intravitreal Pharmacokinetics in Mice: SPECT/CT Imaging and Scaling to Rabbits and Humans. *Mol Pharm.* 2019;16:4399–4404.
51. LeBlanc ME, Wang W, Ji Y, et al. Secretogranin III as a novel target for the therapy of choroidal neovascularization. *Exp Eye Res.* 2019;181:120–126.
52. Schmidt-Erfurth U, Kaiser PK, Korobelnik J-F, et al. Intravitreal aflibercept injection for neovascular age-related macular degeneration: ninety-six-week results of the VIEW studies. *Ophthalmology.* 2014;121:193–201.
53. Balaratnasingam C, Dhrami-Gavazi E, McCann JT, Ghadiali Q, Freund KB. Aflibercept: a review of its use in the treatment of choroidal neovascularization due to age-related macular degeneration. *Clin Ophthalmol.* 2015;9:2355–2371.
54. Nguyen VP, Henry J, Zhe J, et al. Age differential response to bevacizumab therapy in choroidal neovascularization in rabbits. *Exp Eye Res.* 2022;223:109215.
55. Deindl E, Buschmann I, Hofer IE, et al. Role of ischemia and of hypoxia-inducible genes in arteriogenesis after femoral artery occlusion in the rabbit. *Circ Res.* 2001;89:779–786.
56. Schierling W, Troidl K, Troidl C, Schmitz-Rixen T, Schaper W, Eitenmüller UK. The role of angiogenic growth factors in arteriogenesis. *J Vasc Res.* 2009;46:365–374.
57. Wu S, Wu X, Zhu W, Cai W-J, Schaper J, Schaper W. Immunohistochemical study of the growth factors, aFGF, bFGF, PDGF-AB, VEGF-A and its receptor (Flk-1) during arteriogenesis. *Mol Cell Biochem.* 2010;343:223–229.
58. Buschmann I, Schaper W. Arteriogenesis Versus Angiogenesis: Two Mechanisms of Vessel Growth. *Neurophysiol Sci.* 1999;14:121–125.
59. Heil M, Eitenmüller I, Schmitz-Rixen T, Schaper W. Arteriogenesis versus angiogenesis: similarities and differences. *J Cell Mol Med.* 2006;10:45–55.
60. Arras M, Ito WD, Scholz D, Winkler B, Schaper J, Schaper W. Monocyte activation in angiogenesis and collateral growth in the rabbit hindlimb. *J Clin Invest.* 1998;101:40–50.
61. la Sala A, Pontecorvo L, Agresta A, Rosano G, Stabile E. Regulation of collateral blood vessel development by the innate and adaptive immune system. *Trends in Molec Med.* 2012;18:494–501.
62. Ishida S, Usui T, Yamashiro K, et al. VEGF164-mediated inflammation is required for pathological, but not physiological, ischemia-induced retinal neovascularization. *J Exp Med.* 2003;198:483–489.
63. Nagineni CN, Kommineni VK, William A, Detrick B, Hooks JJ. Regulation of VEGF expression in human retinal cells by cytokines: implications for the role of inflammation in age-related macular degeneration. *J Cell Physiol.* 2012;227:116–126.
64. Corliss BA, Azimi MS, Munson JM, Peirce SM, Murfee WL. Macrophages: An Inflammatory Link Between Angiogenesis and Lymphangiogenesis. *Microcirculation.* 2016;23:95–121.